Water microbial disinfection via supported nAg/Kaolin in a fixed-bed reactor configuration

Lütfiye Yıldız Ozer[a,b,1], Ahmed Yusuf[a,b,1], Joao M. Uratani[a,b], Belén Cabal[c], Luis A. Díaz[c], Ramón Torrecillas[c], José S. Moya[c], Jorge Rodríguez[a,b,d,*], Giovanni Palmisano[a,b,d,*]

[a] Department of Chemical Engineering, Khalifa University, P.O. Box 127788, Abu Dhabi, United Arab Emirates.

[b] Center for Membrane and Advanced Water Technology, Khalifa University, P.O. Box 127788, Abu Dhabi, United Arab Emirates

[c] Nanomaterials and Nanotechnology Research Centre (CINN), Consejo Superior de Investigaciones Científicas (CSIC), Universidad de Oviedo (UO), Principado de Asturias (PA), Avenida de la Vega 4-6, 33940 El Entrego, Asturias, Spain

[d] Research and Innovation Center on CO2 and H2 (RICH), Khalifa University, P.O. Box 127788, Abu Dhabi, United Arab Emirates

∗ Corresponding authors.
E-mail addresses: jorge.rodriguez@ku.ac.ae (J. Rodríguez), giovanni.palmisano@ku.ac.ae (G. Palmisano).
[1] Both authors contributed equally

Keywords: Water microbial disinfection, Kaolinite, Silver nanoparticle, Fixed-bed reactor, Kn/nAg composites

Abstract

In this paper we have investigated and demonstrated the antimicrobial capabilities of nano-silver-4 wt%-kaolin (nAg-4-Kn) composite supported on borosilicate glass beads (BGB). Tests have been conducted in a fixed bed reactor on effluent from the secondary clarifier of a conventional wastewater treatment plant (WWTP) in Abu Dhabi, United Arab Emirates (UAE). The prepared BGB with immobilized nAg-4-Kn (nAg-4-Kn/BGB) were characterized using the RAMAN spectroscopy, TEM equipped with EDX and Focus Ion Beam Scanning Electron Microscope (FIB-SEM) techniques. The rate of disinfection was assessed through Luria-Bertani (LB)-agar plate cell counting technique. The results showed complete disinfection after few hours, which was preserved even after several days in repeated runs. The nAg-4-Kn/BGB was reused, demonstrating that the immobilization of nAg-4-Kn was stably achieved, and the activity and integrity of the composites on the BGB were preserved. First order disinfection kinetic constants were estimated to be 2.76 cm h−1 and 2.56 cm h−1 in two consecutive runs. Analyses of the beads after the experiments showed minor losses of nAg from the kaolin matrix thereby corroborating reusability of these materials.

1. Introduction

The global urbanization trend, reflected in geographically densified anthropogenic activities, has been associated with increasing freshwater demand and wastewater generation (Ghosh et al., 2017). Together, these two processes pressure the locally available water supply (both surface and ground aquifers) and might lead to the utilization of alternative water sources such as storm-water, surface runoffs, and treated sewage effluents (TSE) both domestic and industrial. In industrial effluents, potential contamination by various pollutants (e.g. heavy metals, macro-solids, pathogens, soluble and insoluble organic matter, inorganics and nutrients) is a growing concern. The elimination of these undesired constituents before disposal or reuse is becoming more challenging due to the limitations of the conventional treatment technologies, which are stymied by low removal efficiency and inefficacy against emerging pathogens and micro-pollutants. Therefore, there is a need for cost-effective wastewater treatment techniques that can remove a broad range of emerging micro-pollutants and pathogens (Luo et al., 2014; Tilley et al., 2014; Angelakis and Snyder, 2015; Salgot and Folch, 2018). In currently operating wastewater treatment plants (WWTP), disinfection of TSE is expected to occur in tertiary treatment unit operations (Prieto-Rodriguez et al., 2012). The conventional methods used for removal of these micro-organisms are well established, and they include − but are not limited to − chlorination, chloramination, ozonation and ultraviolet treatment. Generally, chlorination is the most commonly used in the WWTPs, and the use of chlorine has become a major environmental issue due to the formation of toxic disinfection byproducts (DBPs). This toxic DBPs include haloacetic acids, trihalomethanes, haloacetonitriles which are toxic to the aquatic organisms (da Costa et al., 2014). Wang et al. (Wang et al., 2007) reported that the toxicity of the wastewater samples increased after chlorine treatment due to the reaction between dissolved organic compounds (DOCs) and chlorine, resulting in the formation of toxic DBPs.

Beside the production of toxic DBPs during the treatment of wastewater, emerging antimicrobial and disinfectant-resistant bacteria in domestic and industrial wastewaters can also limit the treatment capacity of current processes (Primm et al., 2004; Crockett, 2007; Li et al., 2019). Therefore, a materials-property approach to the disinfection of wastewater effluents is a potentially suitable way to develop new treatment technologies. In recent studies, focus has been put on the synthesis of such materials, characterized by: a) low cost, b) high efficiency against recalcitrant micro-organisms, c) low potential for development of microbial resistance, and d) long-term stability (Kim et al., 2007). Organic materials have been widely researched and various studies have consistently reported their limitations which include low resistance to heat, high decomposability and short life span (Cabal et al., 2010; Quintero et al., 2013; Silvestre et al., 2013; Suppakul, 2016).

In view of these setbacks with organic materials, new agents based on inorganic nanomaterials have been gaining a lot of research attention (Fang et al., 2006). The increasing effectiveness of nanotechnology for various applications has raised interest in the antimicrobial properties of metal nanoparticles such as nano-silver (nAg) and nano-copper (nCu) (Pal, 2017). Metal nanoparticles display significant degrees of antimicrobial activity against a broad range of microbial communities due to their promising physicochemical characteristics, including their large specific surface area, crystallographic surface structures and their particle sizes. Among numerous types of nanoparticles, nAg has emerged as one of the most researched antimicrobial active

agents due to its broad-spectrum of antimicrobial activity and its lower tendency to stem microbial resistance than antibiotics (Figoli et al., 2017; Kunduru et al., 2017). The nAg antimicrobial mechanism acts through either the rupturing of cell membranes by interaction of the silver ion (Ag+) with thiol groups in the membrane or through the damaging of the cell membrane upon promoting the formation of the reactive oxygen species (ROS) (Vimbela et al., 2017).

Silver nanoparticles (Ag-NPs) are prevalent in various industrial applications and products, such as antimicrobials, paints, coatings, and food packaging, with a relatively high usage compared to other metals and alkaline earth metals in nanoparticles applications (Brar et al., 2010; Awad et al., 2017; Calderón-Jiménez et al., 2017; Laux et al., 2018; Lee and Jun, 2019). Ag-NPs may enter the wastewater influent stream to be treated at WWTP as a leachate of silver nanoparticlecontaining products, such as textiles. Both human activities (e.g., washing and rinsing) and environmental conditions (e.g. raining) can release the Ag-NPs. While the biologically-active microbial community is expected to cope with such particles in the treatment vessels, due to the formation of suspended flocs or biofilms (Sheng and Liu, 2011), Ag- NPs can interact with the conventional disinfection process in WWTP (Yuan et al., 2013).

The fate of such Ag-NPs in the environment is a growing field of
research, accompanying the increase in their industrial applications. Wastewater sludge contamination by nanoparticles boosts the concerns on their environmental toxicity and related effects (Brar et al., 2010; Gottschalk et al., 2013; Yang et al., 2013; Wang et al., 2016). The presence of Ag-NPs may impact the suitability of biosolids (a bye-product of WWTP) reuse in agricultural applications, due to the potential risk of nanoparticle leachability into ground- and sub-surface water bodies. Biotoxicity of Ag-NPs is directly related to their stability in environmental conditions, which is affected by pH, ionic components and strength, dissolved concentration of oxygen and sulfide, light, type of coating material, clays, bio-colloids, and kind (fulvic acid and humic acid) and source (soil and water) of natural organic matter (Sharma et al., 2014). By immobilizing the nanoparticles in clay-based matrix, the resulting nanocomposites can be used as a functional development of novel disinfection treatments (Tran et al., 2013), which can lessen their impact on WWTP biosolids.

A known limitation in the practical applications of nAg is its propensity to agglomerate in aqueous medium, which progressively diminishes its efficiency over time (Lu et al., 2016). nAg impregnated on adsorbent materials can overcome this limitation and provides a promising alternative to the use of nAg powder combined with a stabilizer. Many researches focused on the stabilization of nAg on adsorbent materials, including cellulose fiber (Dankovich and Gray, 2011), polyethersulfone microfiltration membranes (Ferreira et al., 2015), montmorillonite (Magaña et al., 2008), and activated carbon (Gonçalves et al., 2016). Although some adsorbent materials such as activated carbon actively contribute to the reduction of bacterial growth (Escherichia coli), they were found to be toxic to aquatic organisms like Hydra attenuata and also to plants (Lycopersicum esculentum) (Gonçalves et al., 2016). Thus, the selection of the adsorbent material is critical to minimize undesired environmental effects.

Clay minerals are excellent adsorbent materials, which can be used to avoid the leaching of the Ag-NPs into the TSE. They are relatively abundant in nature, with low cost, relatively low toxicity, high surface area leading to the excellent sorption capacity, antimicrobial properties compared with non-clay minerals (Unuabonah et al., 2018).

Many clays, with antimicrobial properties, reported in the literature, usually contain Fe, Fe–smectite, disordered illite/smectite, 1 M illite/smectite with R2 ordering (Williams et al., 2011; Williams, 2017). The combination of antimicrobial clay with other transition metals (Zn, Mn, Ni, Cu, Co) can also create toxic condition for pathogens (Londono et al., 2017). The particle size and pH of the reaction environment was found to greatly affect the antimicrobial activity of clay. According to a study by Williams (Williams, 2017), French green clay (mainly consisting of two type of illite, one-disordered (1 Md) an 1 millite-smectite with R2 ordering) possesses antimicrobial activity when the particle size was less than 200 nm and it has no activity when the size is larger than this. Phrophyllite, an antimicrobial clay, facilitates adhesion to microorganism or pathogens by surface attraction in order to hinder the uptake of essential nutrients, disrupts cell envelopes or weakens efflux of metabolites (Albengres et al., 1985; Hu and Xia, 2006; Williams et al., 2011). In addition, phrophyllite might produce free radicals that induce the degradation of cell membrane. Fe-smectites (hectorite (SHCa-1), nontronites (NAu-1) and nontronites (NAu-2)) have been suggested to induce production of free radicals that lead to lipid peroxidation in bacterial cell membrane (Kibanova et al., 2009).

Kaolinite ($Al_2SiO_5(OH)_4$) is a clay mineral which belongs to the phyllosilicates. It consists of repeating layer of both Al octahedral sheets (gibbsite facet) and Si tetrahedral sheets (silica facet), bound to each layer by hydrogen and dipolar bonds. The surface charge of kaolin is heterogenous and anisotropic due to the different substitution degree and type on the basal plane. On the other hand, its edge charge depends on the pH of the solution. The properties of kaolinite in aqueous solutions have been intensively studied due to its relative abundance in nature, low cost, chemical and structural stability. The physicochemical and mechanical properties depend on its particle size, surface area and crystallinity, determined by the stacking order of the each layer of kaolinite (Bolland et al., 1976; Brady et al., 1996; Kumar et al., 2016; Awad et al., 2017). Kaolinites have been shown to possess appreciable disinfecting capabilities (Unuabonah et al., 2018), hence compositing with nAg increases the antimicrobial action of the resulting materials. Apart from enhancing antimicrobial properties of nAg, the stability of nAg is also positively affected, thereby increasing the bio-compatibility. Previous studies have indicated that nAg immobilized on the solid matrix shows a broad range and effective antimicrobial properties and low cell cytotoxicity (Su et al., 2011; Lin et al., 2013; Unuabonah et al., 2018). As promising as kaolin-nAg composites are, kaolin (mainly with particle size smaller than 25 µm and in the form of flat-shaped particles) is stymied by difficulty in recovery from aqueous solution which makes it hard to be applied in microbial disinfection plants (Barani and Kalantari, 2018). The separation of kaolin in industry is mostly carried out by overflow through hydro-cyclones. It was found that following 4th or 5th hydro-cyclones steps, remaining kaolin particles cannot be isolated in the disinfection plant (Köster et al., 1992; Yuehua et al., 2004; Barani and Kalantari, 2018).

In order to circumvent this limitation, in this work kaolin-nAg was supported on glass beads and arranged in a fixed bed reactor setup to evaluate its antimicrobial capabilities using a real wastewater effluent. The prepared material, characterized using Raman and Focus Ion Beam Scanning Electron Microscope (FIB-SEM) was evaluated for water antimicrobial capabilities. To the best of our knowledge, no study has shown the use of this composite supported on glass beads and arranged in a fixed bed reactor configuration. This set-up greatly reduces the potential toxicity of nAg due to increased stability when immersed in water.

2. Experimental procedure

2.1 Materials

Kaolin was supplied by CAVISA, La Coruña, Spain. All other chemicals (AgNO3, Dolapix CE-64, Triton X-100, acetone, ethanol, nitric acid, bacterial agar, peptone, tryptone, NaCl, yeast extract, and LBagar) were supplied by Sigma Aldrich. Elemental analysis of the used kaolin was determined by wavelength dispersive X-ray fluorescence spectrometry (XRF) (SRS 3000 Bruker). The chemical composition (% w/w) of kaolin was: 59.4 SiO2, 33.1 Al2O3, 0.16 TiO2, 0.40 Fe2O3, 0.24 CaO, 0.31 K2O, 6.16 LOI, 0.23 others. Treated wastewater samples were obtained from the secondary clarifier of a conventional domestic wastewater treatment plant located in Abu Dhabi, United Arab Emirates.

2.1.1 Characterization of kaolin powders

The XRD analyses of the powder samples were carried out in a Bruker D8 Advance diffractometer using CuKα radiation at 40 kV and 30 mA in a step-scanning mode from 4o to 70o with a step width of 0.05o and a step time of 0.5 s. The real densities of the kaolin and the kaolin with silver nanoparticles were measured in a Micromeritics Accupyc 1330 helium gas pycnometer. N2 isotherms at −196 °C were recorded using a Micromeritics ASAP 2420. The samples were degassed under vacuum at 120 °C prior to the adsorption measurements. The specific surface areas were calculated using the BET method from the adsorption isotherms within the relative pressure (p/p0) range 0–0.27.

2.2 Preparation process

The nAg-4-Kn powder was prepared in a similar way to that described by Cabal et al. (Cabal et al., 2010), but following an easily scalable procedure. The nAg-4-Kn composites were prepared from both kaolin and silver precursors using thermal reduction. An aqueous kaolin suspension was prepared and a dispersant (Dispex N40) was added to stabilize and homogenize the resulting suspension, followed by dropwise addition of a silver precursor (AgNO3) solution with the appropriate concentration to yield a final 4 wt% in silver. This suspension was stirred with an overhead stirrer for 24 h. Rheological analysis was performed in a Ford cup number 4 (viscosity of the suspension: 47.04 cP). The resulting suspension was then atomized in a pilot scale spray dryer (Niro Mobile Minor™). Inlet and outlet air temperatures were respectively 150 and 70 °C, and the feeding velocity was 1.2 L h−1. The thermal reduction was carried out by calcining the resulting material at 350 °C for 2 h in air atmosphere.

The nAg-4-Kn powder was immobilized on borosilicate glass spherical beads (diameter ca. 3 mm) after optimizing the composition of the used suspension and the treatment procedures, as described in the following. Prior to deposition, the beads were cleaned with acetone and ethanol in two consecutive 10 min steps under ultrasound treatment and then washed with deionized water under vacuum condition. A 15 mL suspension, containing 0.6 g of nAg-4-Kn powder, 14.92 mL of ethanol (organic solvent where the powder is suspended effectively), 315 µL of Triton X-100 (nonionic surfactant agent) and 0.5 µL of nitric acid (stabilizer agent) were deposited using a spray pen gun equipped with a cylindrical needle nozzle with a diameter of ca. 0.35 mm (VALEX, Italy) under 2 bar air pressure at room temperature for around 2 min by using 600 beads (weight: ca.

45 g) and keeping the nozzle at a distance of 8 cm. After deposition, the nAg-4-Kn coated beads were annealed applying the following steps: heating up to 50 °C in 30 min, heating up from 50 °C to 450 °C in 6 h, 4 h at 450 °C, and cooling down below 200 °C in 2 h. This deposition and annealing step were repeated ten times. Afterwards, the beads were sprayed with the solution containing ethanol, Triton X-100 and nitric acid without nAg-4-Kn powder, then annealed in the same conditions. Finally, the beads were washed with deionized water until no leaching of nAg-4-Kn powder was detected and then dried in an oven for 30 min at 50 °C.

2.3. Characterization of powder immobilized on beads

Raman spectroscopy was applied to identify the crystal phases present in the films deposited on the beads. Raman was conducted in a confocal Raman spectroscope (Alpha 300R from Witec) and the film was excited with a 532 nm laser having a single mode output power of 52 mW.
Cross-sectional and surface morphology of the samples were investigated by Focus Ion Beam Scanning Electron Microscope (FIB-SEM, Helios NanoLab). Sample was mounted on a stainless-steel stub by using silver paste and coated with 30 nm gold. SEM stage was tilted to 52 °C and the ion beam current was 20 nA to etch the rectangular sample with 20 µm length, 10 µm width, 10 µm depth in size. Then the cross section was cleaned with a 100-pA ion beam. TEM analysis was conducted by using a Tecnai G2 transmission electron microscope, operating at 200 kV and equipped with EDX to analyze the film deposited on the beads before and after activity runs.

2.4 Assessment of water disinfection

The antimicrobial effect of the nAg-4-Kn powder immobilized on borosilicate beads was evaluated on water collected from a conventional domestic wastewater treatment plant from Abu Dhabi. Water from the supernatant of the WWTP secondary clarifiers was diluted 1:1000 down to low bacterial cell concentration values in order to study the immobilized nAg-4-Kn disinfection kinetics under unsaturated conditions. It can be envisaged that dilution will not be needed in scaled-up systems and, in fact, it was used in the present lab-scale set-up for analytical convenience. Both positive and negative controls were prepared: positive controls included treated water (TW) only and treated water (TW)/bare borosilicate glass beads (BGB), while negative control samples included milli Q water and a sterilized LB agar plate.
A scheme of the experimental setup utilized for the disinfection experiments is shown in Fig. 1. The experimental runs were carried out at room temperature (ca. 24 °C) by using 60 mL mini-reactors, purposely built using plastic syringes and operated in a mixed batch mode with a high recirculation of 10 mL min−1 provided by a multi-channel pump. Each mini-reactor contained ca. 100 BGB, and Samples of 300 µL were collected from 0 to 12 and 24 h from the reactors to monitor the cell count.
Microbial disinfection assessment was conducted using plate cell counting on LB-agar. The plate culture media, containing 10 g L−1 tryptone (essential amino acid source), 5 g L−1 NaCl, 5 g L−1 yeast extract (nutrient source) and 15 g agar L−1 (solid substrate) were autoclaved at 121 °C for 15 min and poured in the sterile Petri dishes. 100 µL of each sample and control samples were inoculated in LB-agar plates and incubated at 37 °C

for 24 h. The serial dilution method was utilized to achieve higher confidence numbers of the bacterial colonies described as colony forming units (CFU) per mL.

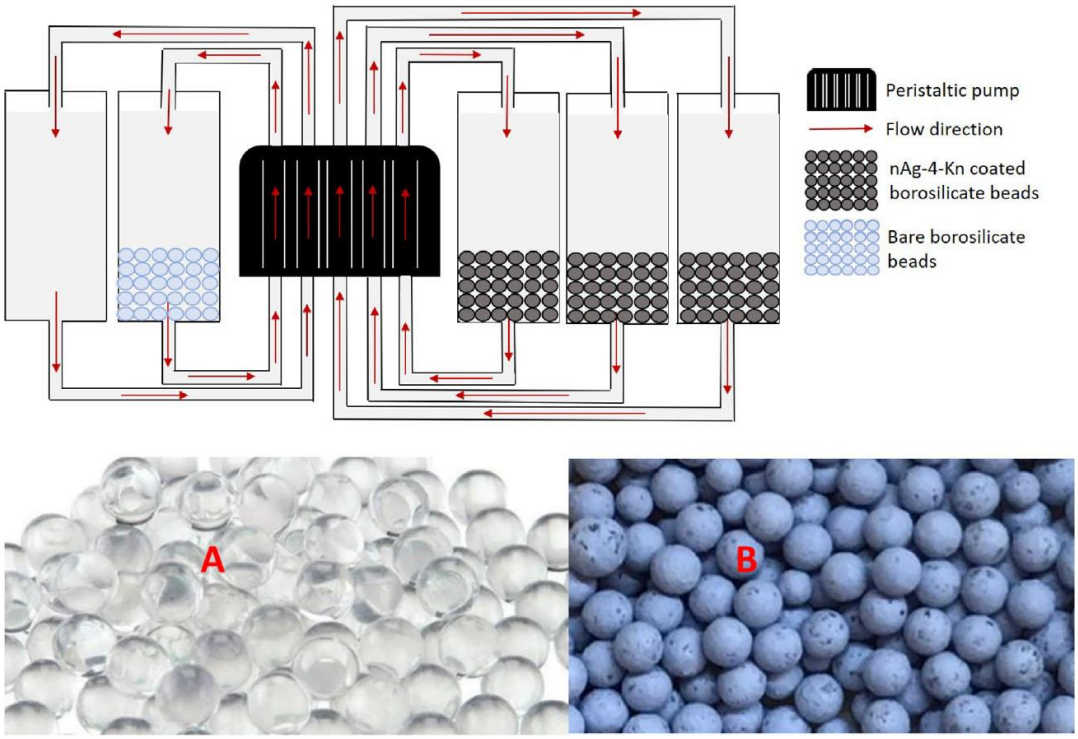

Fig. 1. Scheme of the experimental setup used to evaluate the antimicrobial capabilities of the different materials, the mini-reactors operate as batch under high mixing provided by the full recirculation pump (top). Pictures of the bare BGB (A, bottom) and nAg-4-Kn supported on BGB (B, bottom).

3. Results & discussion

3.1. Characterization

Mineral identification was confirmed by XRD (see Fig. 2), kaolinite (PDF 78–2110) and quartz (PDF 65-0466) were recognized as the constituents of the used kaolin. On the other hand, metallic silver Bragg reflection (PDF 87-0717) is clearly visible in the kaolin with silver nanoparticles (nAg-4-Kn). The adsorption/desorption N2 isotherms are shown in Fig. 3. According to the classification of the International Union of Pure and Applied Chemistry (IUPAC) (Sing et al., 1985), the isotherms of both samples are of type IV which is associated with capillary condensation in mesopore structures. The hysteresis loop of these samples is similar to type H3, typical of agglomerates of plate-like particles containing slit-shaped pores. This pore format is consistent with the lamellar structure of kaolin. The incorporation of silver nanoparticles to kaolin matrix does not affect the real density of kaolin (2.8 g cm-3) whereas the specific surface area decreases due to the surface occupied by nAg and the shrinking of pores after the thermal treatment undergone following nAg deposition (SBET kaolin: 18 m2 g-1 and SBET nAg-4Kn: 10 m2 g-1).

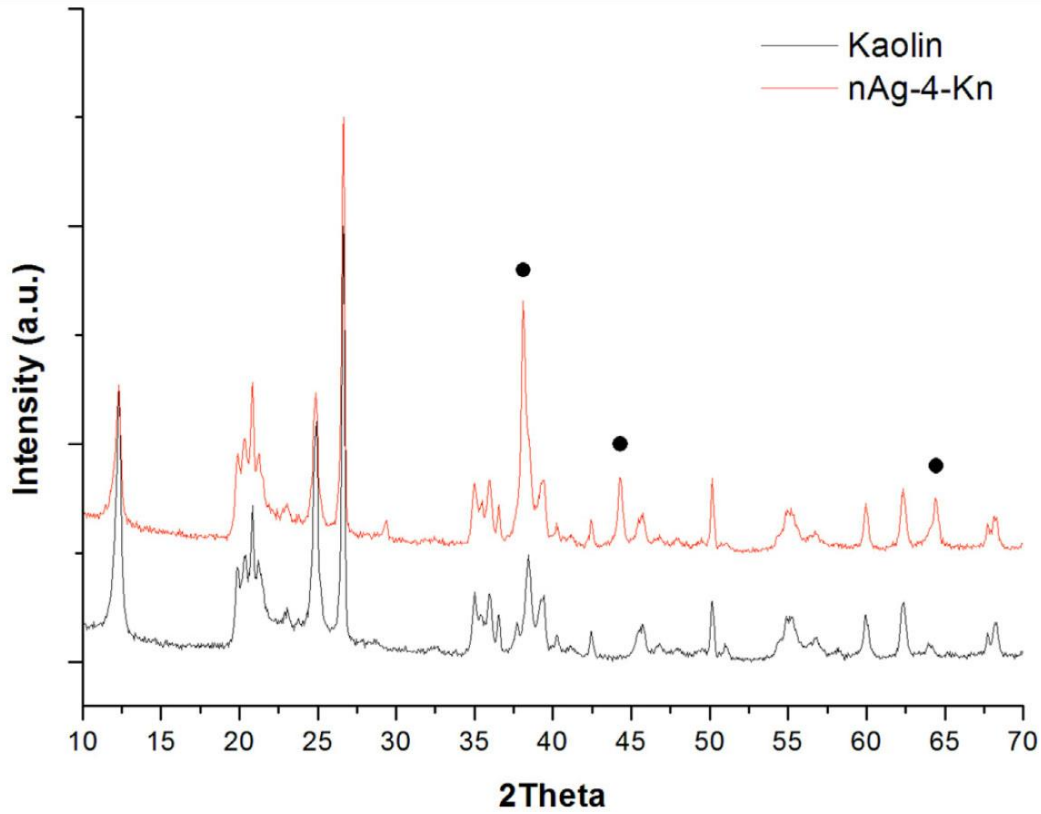

Fig. 2. XRD of kaolin and nAg-4-Kn. Peaks attributed to metallic silver are labelled with black dots.

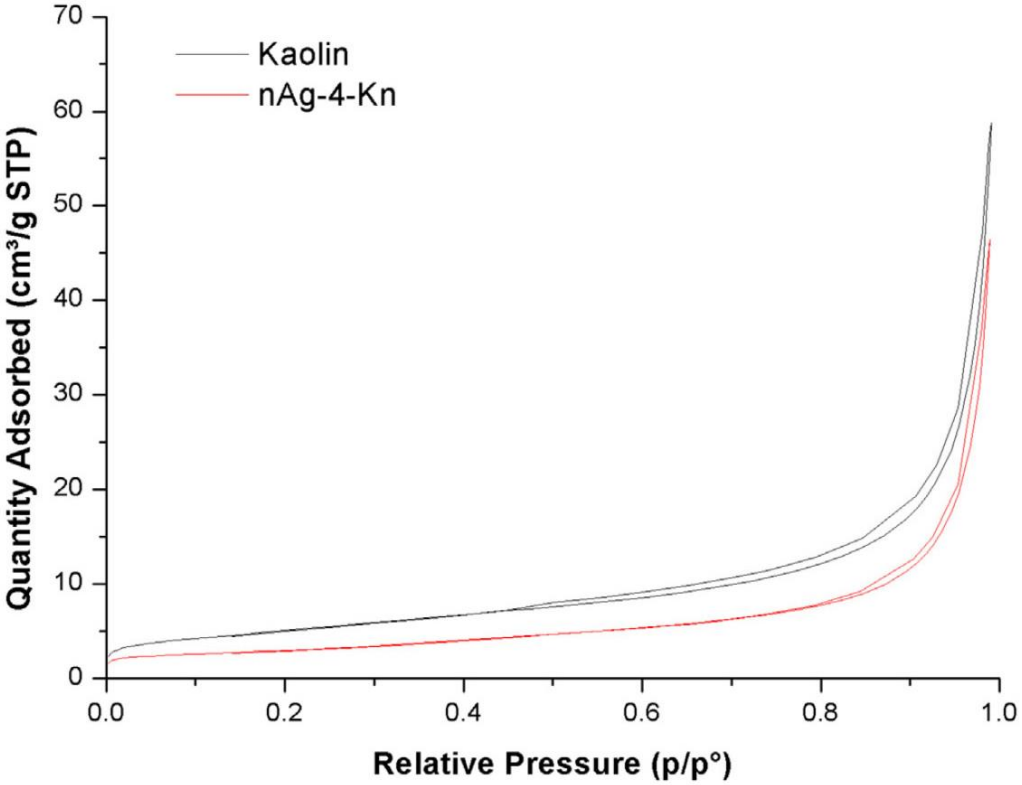

Fig. 3. N2 adsorption/desorption isotherms of kaolin and nAg-4-Kn. (For interpretation of the references to color in this figure legend, the reader is referred to the web version of this article.)

After achieving the immobilization of nAg-4-Kn powder on BGB, the resulting material was detached from BGB by ultrasound treatment in 2-propanol, and analyzed at the TEM. Fig. 4 shows images of the powder detached from BGB, where nAg appears monodistributed on a kaolin matrix. TEM imaging and EDX were run before (A) and after (B) use in activity tests. It can be noticed how Ag-NPs are anchored homogenously pointing to the preservation of their morphology after immobilization took place. The successful and homogeneous immobilization of nAg is related to the reduction of silver on preferential adsorption sites (i.e. hydroxyl groups), as previously reported (Cabal et al., 2010). EDX analysis showed the presence of silicon, oxygen, aluminum, silver, deriving from the substrate and a small difference was observed between the measured Ag loading of unused (3.55 wt%) and used (3.12 wt%) materials. Although this difference (0.43 wt%) is not high with respect to the limited sensitivity of EDX, it can be tentatively ascribed to a minor leaching of silver into the solution. Fig. 4D shows the highly porous surface of nAg-4-Kn immobilized on BGB, which offers a large platform during wastewater microbial disinfection.

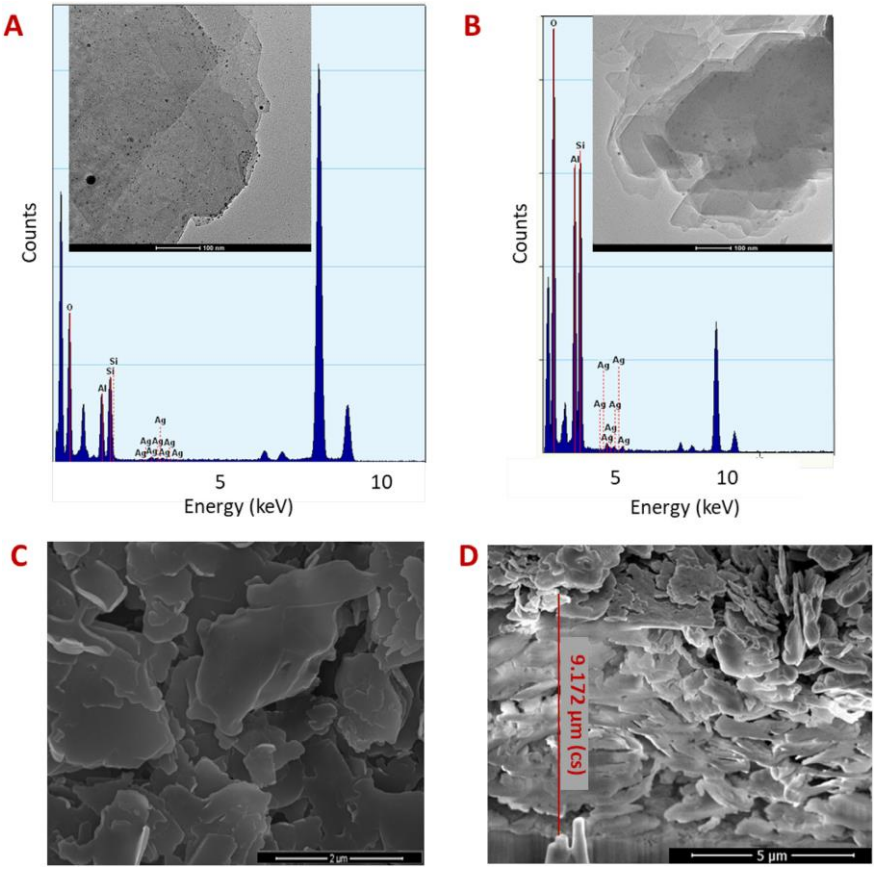

Fig. 4. TEM-EDX (A and B, bar: 100 nm) and SEM and FIB-SEM (C and D) images of nAg-4-Kn immobilized on borosilicate glass beads. TEM-EDX analysis was carried out by detaching the powder from used (A) and unused (B) beads. A cross-sectional SEM image obtained after etching the sample through Focus Ion Beam (FIB) confirmed that the sample is mostly macro-porous, as shown in the profile micrograph reported in Fig. 4C. The red line (Fig. 4D) indicates that the thickness of nAg-4- Kn supported on the beads is ca. 9 µm.

Fig. 5 depicts the Raman spectra of the nAg-4-Kn supported on BGB and of bare BGB before and after the activity tests. The Raman spectra obtained from nAg-4-Kn supported on BGB did not exhibit the characteristic peaks of Kn between 3600 cm−1 and 3700 cm−1 corresponding to the vibration of the OH– groups in its structure, as

indicated in literature (Frost and Kloprogge, 2001), due to the size of its crystalline structure. Moreover, the Raman spectra of nAg-4-Kn supported on beads indicated that the background intensity was much lower after the experiment. This might be associated with a minor loss of powder during the experiment, as supported in TEM-EDX result, which, however, did not compromise the BGB activity as shown in the following sections. The bare BGB Raman spectrum displayed additional peaks after the experiment, which can come as a result of formation of a biofilm on the bare BGB, which is not active against microorganism buildup (Fig. 5) (Pahlow et al., 2015; Scandura et al., 2017). In particular, the two additional peaks, appearing at ca. 1350 and 1575 cm−1 could be due to the δ (C–H) deformation vibration, and δ (NH) deformation and ν (CN) stretching vibration, respectively. These peaks might have appeared due to the amino acid sequence in the peptidoglycan, as previously reported (Williams and Edwards, 1994).

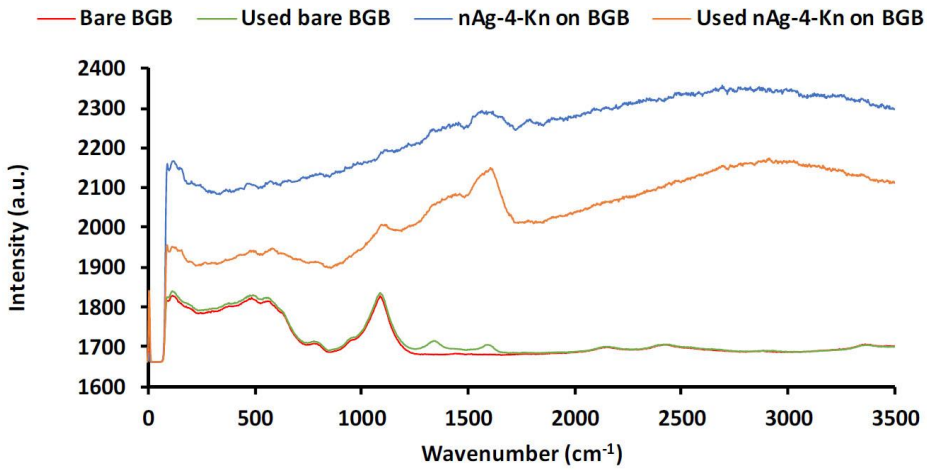

Fig. 5. Raman spectra of: unused (red) and used (green) bare BGB; unused (blue) and used (orange) nAg-4-Kn supported on BGB. (For interpretation of the references to colour in this figure legend, the reader is referred to the web version of this article.)

3.2. Antimicrobial capability and kinetics

The antimicrobial effect of the monodistributed nAg supported on a kaolin matrix and immobilized on BGB was investigated by counting viable cell colonies after exposure of the water samples to these nAg-4- Kn/BGB arranged in a fixed-bed disinfection batch mini-reactors operating at 25 °C for 24 h. From Fig. 6, it is evident that after 1 h, nAg-4-Kn/BGB reduced the number of viable microorganisms in the clarified water and, after 2 h, no viable cells were observed for as long as 24 h. As for the TW/BGB control, a slight decrease in the viable microorganisms' number was observed in the first 8 h due to biofilm formation on bare BGB and after 8 h this control sample had no decrease in the viable cell number. These results indicate that nAg-4-Kn produces an antimicrobial effect as indicated in literature (Kowalska-Góralska et al., 2015; Küünal et al., 2016) and this property is maintained after the immobilization on beads thanks to the preservation of nAg dispersion and the high porosity exhibited by the supported material, which assured a substantial activity. Notably, the nAg-4-Kn immobilized on BGB was washed after experiment and reused without any significant drop in activity. The results (see Fig. 7A) indicated that the beads can be reused without any significant change in their

antimicrobial properties, testifying the stability of nAg-4-Kn supported on the glass beads, without any need to recover the material from the treated water. The antimicrobial activity in the second experimental window of 24 h was highly similar to that of the first run, whereby there was no observable viable colonies after 2 h. In Fig. 7B, the results of a longer experiment (288 h) starting at higher microbial concentration are shown to validate the long-term usability of the nAg-4-kn/BGB as well as its biocidal characteristics. The antimicrobial activity of Ag is proposed to occur mainly through two pathways: (1) the loss of cell membrane integrity due to the interaction with Ag and cell membrane protein and (2) the formation of ROS leading to oxidative stress and cell lysis (Vimbela et al., 2017). The antimicrobial activity of Ag depends on the size, the surface area and the surface structure. According to the previous studies, smaller nanoparticles have higher antimicrobial properties (Zhou et al., 2012; Chernousova and Epple, 2013). The immobilization of Ag on kaolin results in a high exposed surface area of Ag, leading to a strong antimicrobial effect on wastewater.

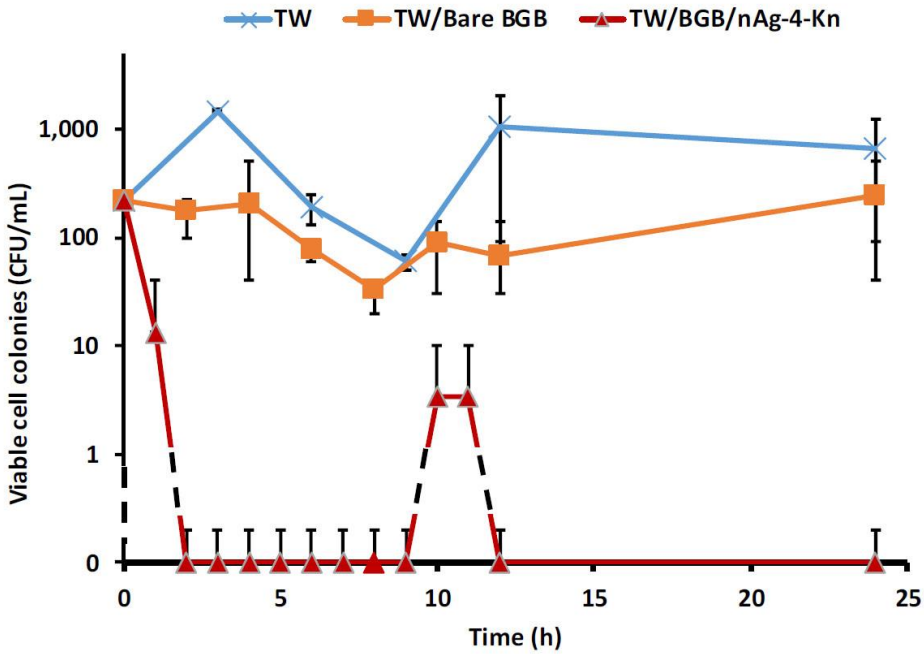

Fig. 6. Antimicrobial activity of the kaolin-4-nAg composites immobilized on BGB using collected water samples; controls include inoculum only (TW) and inoculum containing bare BGB (TW/Bare BGB). (TW = inoculum, BGB = borosilicate beads).

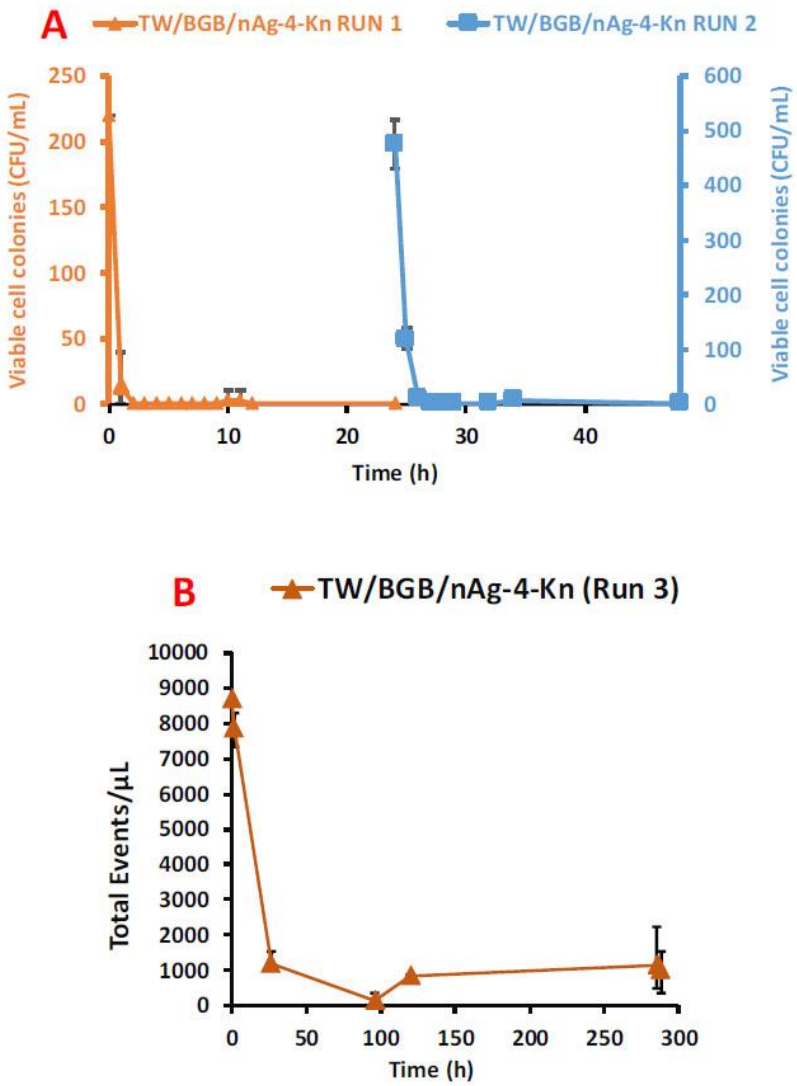

Fig. 7. Reusability test for the nAg-4-Kn immobilized on BGB: (A) two consecutive runs of 24 h each, and (B) long experimental run of 288 h at higher microbial concentration. (TW = inoculum, BGB = borosilicate beads).

It is worthy to note that the disinfection test was carried out in an unsaturated condition to avoid bead biofouling. Although this might not be totally representative of real applications, the major aim was to demonstrate the antimicrobial capabilities of this material supported on glass beads. Further development will be aimed at the use of a larger scale fixed bed reactor able to handle undiluted wastewater with sections of the bed working under saturated conditions.

3.3. Kinetics of disinfection

Based on the results obtained from Fig. 7A, we propose the disinfection rate to be pseudo-first order; therefore, we estimated the rate to follow (Eq. (1)):

$$R_d = \frac{\mathrm{dC}}{\mathrm{dt}} = -k_d \mathrm{A_s} C$$

where C (CFU mL-1) refers to the viable colonies at time t (h), As (cm−1) the active surface area of beads per unit volume of reaction, Rd is the disinfection rate in CFU mL-1 h-1 and kd is the area specific first order kinetic constant in cm h−1. To estimate the kinetic constant, Eq. (1) was integrated with initial condition: t=0, C0 = 220 and 475 CFU mL-1, as shown in Fig. 7A and Eq. (2) was obtained.

$$-\log_{10}\frac{C}{C_o} = (\log_{10} e \times (k_d A_s)) \times t$$

By fitting the model to the experimental data, we obtained the value of the rate constant as shown in Fig. 8. The value of the decay rate (kdAs) is quite similar in both cases, run 1 has a rate of 2.127 h−1 with r2 = 0.8625 and run 2 has a rate of 1.972 h−1 with r2 = 0.9823. These constants are close to each other, and the actual kd can be estimated by dividing by the active surface area of beads per unit volume of reaction (As). This similarity in the run 1 and run 2 is also expected since first order kinetics were proposed. The volume of reaction was 50 mL and, on average, the estimated surface area for each bead is 0.385 cm2. Since 100 beads were used in the runs, the estimated total surface area was 38.5 cm2. From these values, kd was estimated to be 2.76 cm h−1 (for run 1) and 2.56 cm h−1 (run 2).

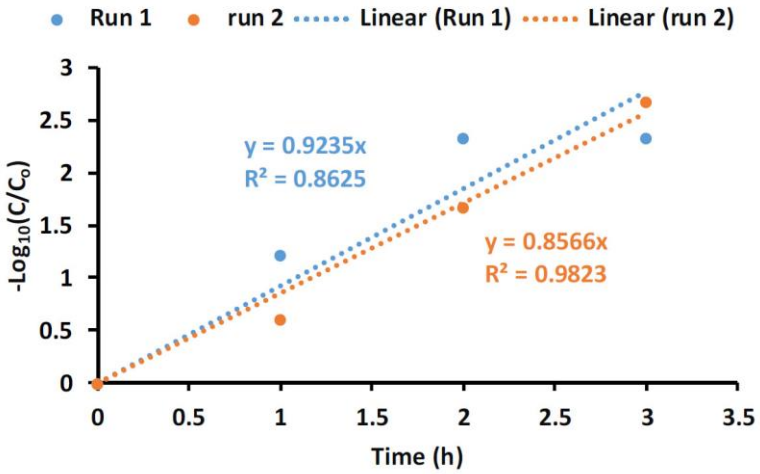

Fig. 8. Fitting of the experimental data to a linear model: y is representing (−Log10(C/Co)) and x is reaction time as shown in Eq. (2).

4. Conclusion

The antimicrobial effect of the nAg-4-Kn immobilized on BGB has been investigated in a fixed-bed configuration applied to clarified water samples from a conventional domestic wastewater plant (Abu Dhabi, UAE). The LB-agar plate counting technique was applied for cell counting quantification. Appropriate negative and positive controls have been used to verify obtained results. The experiment was also carried out under unsaturated conditions with low initial bacteria cell concentration to avoid biofouling. The results obtained showed that nAg-4-Kn composite has strong antimicrobial capabilities, and no viable microbial colonies were observable after few hours. Proposed first order rate fits with the experimental data, and a first order rate of 2.76 cm h−1 and 2.56 cm h−1 were

obtained in two different runs. The second run demonstrated also that the nAg-4-Kn immobilized on BGB is reusable even by doubling initial microbial concentration. Characterization techniques showed slight leaching of the immobilized powder from the beads but the integrity of the beads was not affected even after activity. Overall, the nAg-4-Kn suitability as a possible antimicrobial material has been demonstrated and further study could lead to its application as large scale disinfection alternative in wastewater treatment or other domestic or industrial antimicrobial applications.

Declaration of Competing Interest

The authors declare that they have no known competing financial interests or personal relationships that could have appeared to influence the work reported in this paper.

Acknowledgment

Authors are grateful to Susana Martinez from Nanomaterials and Nanotechnology Research Center (CINN) for providing excellent technical assistance.
Lakshmi Satish and Salim Alnaqbi are acknowledged for experimental activity carried out during their internship in Khalifa University. Cyril Aubry, James McElhinney, Ayesha AlMarzooqi, Ahmed F. Yousef and Hector Hernandez are acknowledged for allowing access to equipment and providing support in one of the experimental runs.

References

- Albengres, E., Urien, S., Tillement, J.P., Oury, P., Decourt, S., Flouvat, B., Drieu, K., 1985. Interactions between smectite, a mucus stabilizer, and acidic and basic drugs. Eur. J. Clin. Pharmacol. 28, 601–605. https://doi.org/10.1007/BF00544074.
- Angelakis, A., Snyder, S., 2015. Wastewater Treatment and Reuse: past, present, and Future. Water 7, 4887–4895. https://doi.org/10.3390/w7094887.
- Awad, M.E., López-Galindo, A., Setti, M., El-Rahmany, M.M., Iborra, C.V., 2017. Kaolinite in pharmaceutics and biomedicine. Int. J. Pharm. 533, 34–48. https://doi.org/10.1016/j.ijpharm.2017.09.056.
- Barani, K., Kalantari, M., 2018. Recovery of kaolinite from tailings of Zonouz kaolinwashing plant by flotation-flocculation method. J. Mater. Res. Technol. 7, 142–148. https://doi.org/10.1016/j.jmrt.2017.05.010.
- Bolland, M., Posner, A., Quirk, J., 1976. Surface charge on kaolinites in aqueous suspension. Soil Res. 14, 197. https://doi.org/10.1071/SR9760197.
- Brady, P.V., Cygan, R.T., Nagy, K.L., 1996. Molecular controls on kaolinite surface charge. J. Colloid Interface Sci. 183, 356–364. https://doi.org/10.1006/jcis.1996.0557.
- Brar, S.K., Verma, M., Tyagi, R.D., Surampalli, R.Y., 2010. Engineered nanoparticles in wastewater and wastewater sludge - evidence and impacts. Waste Manag. 30, 504–520. https://doi.org/10.1016/j.wasman.2009.10.012.
- Cabal, B., Torrecillas, R., Malpartida, F., Moya, J.S., 2010. Heterogeneous precipitation of silver nanoparticles on kaolinite plates. Nanotechnology 21, 475705. https://doi.org/10.1088/0957-4484/21/47/475705.

- Calderón-Jiménez, B., Johnson, M.E., Montoro Bustos, A.R., Murphy, K.E., Winchester, M.R., Vega Baudrit, J.R., 2017. Silver Nanoparticles: technological advances, societal impacts, and metrological challenges. Front. Chem. 5. https://doi.org/10.3389/fchem.2017.00006.
- Chernousova, S., Epple, M., 2013. Silver as antibacterial agent: ion, nanoparticle, and metal. Angew. Chemie 52, 1636–1653. https://doi.org/10.1002/anie.201205923.
- Crockett, C.S., 2007. The role of wastewater treatment in protecting water supplies against emerging pathogens. Water Environ. Res. 79, 221–232. https://doi.org/10.2175/106143006x111952.
- da Costa, J.B., Rodgher, S., Daniel, L.A., Espíndola, E.L.G., 2014. Toxicity on aquatic organisms exposed to secondary effluent disinfected with chlorine, peracetic acid, ozone and UV radiation. Ecotoxicology 23, 1803–1813. https://doi.org/10.1007/s10646-014-1346-z.
- Dankovich, T.A., Gray, D.G., 2011. Bactericidal paper impregnated with silver nanoparticles for point-of-use water treatment. Environ. Sci. Technol. 45, 1992–1998. https://doi.org/10.1021/es103302t.
- Fang, M., Chen, J.H., Xu, X.L., Yang, P.H., Hildebrand, H.F., 2006. Antibacterial activities of inorganic agents on six bacteria associated with oral infections by two susceptibility tests. Int. J. Antimicrob. Agents 27, 513–517. https://doi.org/10.1016/j.ijantimicag.2006.01.008.
- Ferreira, A.M., Roque, É.B., da Fonseca, F.V., Borges, C.P., 2015. High flux microfiltration membranes with silver nanoparticles for water disinfection. Desalin. Water Treat. 56, 3590–3598. https://doi.org/10.1080/19443994.2014.1000977.
- Figoli, A., Dorraji, M.S.S., Amani-Ghadim, A.R., 2017. Application of nanotechnology in drinking water purification. In: Grumezescu, A.M. (Ed.), Water Purification. Elsevier, pp. 119–167. https://doi.org/10.1016/B978-0-12-804300-4.00004-6.
- Frost, R.L., Kloprogge, J.T., 2001. Towards a single crystal Raman spectrum of kaolinite at 77 K. Spectrochim. Acta 57, 163–175. https://doi.org/10.1016/S1386-1425(00) 00345-0.
- Ghosh, A., Nayak, A.K., Pal, A., 2017. Nano-particle-mediated wastewater treatment: a review. Curr. Pollut. Rep. 3, 17–30. https://doi.org/10.1007/s40726-016-0045-1.
- Gonçalves, S.P.C., Strauss, M., Delite, F.S., Clemente, Z., Castro, V.L., Martinez, D.S.T., 2016. Activated carbon from pyrolysed sugarcane bagasse: silver nanoparticle modification and ecotoxicity assessment. Sci. Total Environ. 565, 833–840. https://doi.org/10.1016/j.scitotenv.2016.03.041.
- Gottschalk, F., Sun, T., Nowack, B., 2013. Environmental concentrations of engineered nanomaterials: Review of modeling and analytical studies. Environ. Pollut. 181, 287–300. https://doi.org/10.1016/j.envpol.2013.06.003.
- Hu, C.-H., Xia, M.-S., 2006. Adsorption and antibacterial effect of copper-exchanged montmorillonite on Escherichia coli K88. Appl. Clay Sci. 31, 180–184. https://doi.org/10.1016/j.clay.2005.10.010.

- Kibanova, D., Nieto-Camacho, A., Cervini-Silva, J., 2009. Lipid peroxidation induced by expandable clay minerals. Environ. Sci. Technol. 43, 7550–7555. https://doi.org/10. 1021/es9007917.
- Kim, J.S., Kuk, E., Yu, K.N., Kim, J.H., Park, S.J., Lee, H.J., Kim, S.H., Park, Y.K., Park, Y.H., Hwang, C.Y., Kim, Y.K., Lee, Y.S., Jeong, D.H., Cho, M.H., 2007. Antimicrobial effects of silver nanoparticles. Nanomed. Nanotechnol. 3, 95–101. https://doi.org/10.1016/j.nano.2006.12.001.
- Köster, R., Schreck, B., von Rybinski, W., Dobiás, B., 1992. New reagent systems for the flotation of kaolinite. Miner. Eng. 5, 445–456. https://doi.org/10.1016/0892-6875(92)90224-W.
- Kowalska-Góralska, M., Senze, M., Polechoński, R., Dobicki, W., Pokorny, P., Skwarka, T., 2015. Biocidal properties of silver-nanoparticles in water environments. Polish J. Environ. Stud. 24, 1641–1647. https://doi.org/10.15244/pjoes/39554.
- Kumar, N., Zhao, C., Klaassen, A., van den Ende, D., Mugele, F., Siretanu, I., 2016. Characterization of the surface charge distribution on kaolinite particles using high resolution atomic force microscopy. Geochim. Cosmochim. Acta 175, 100–112. https://doi.org/10.1016/j.gca.2015.12.003.
- Kunduru, K.R., Nazarkovsky, M., Farah, S., Pawar, R.P., Basu, A., Domb, A.J., 2017. In: Grumezescu, A.M. (Ed.), 2 - Nanotechnology for water purification: applications of nanotechnology methods in wastewater treatment. Academic Press, pp. 33–74. https://doi.org/10.1016/B978-0-12-804300-4.00002-2.
- Küünal, S., Kutti, S., Rauwel, P., Guha, M., Wragg, D., Rauwel, E., 2016. Biocidal properties study of silver nanoparticles used for application in green housing. Int. Nano Lett. 6, 191–197. https://doi.org/10.1007/s40089-016-0186-7.
- Laux, P., Tentschert, J., Riebeling, C., Braeuning, A., Creutzenberg, O., Epp, A., Fessard, V., Haas, K.-H., Haase, A., Hund-Rinke, K., Jakubowski, N., Kearns, P., Lampen, A., Rauscher, H., Schoonjans, R., Störmer, A., Thielmann, A., Mühle, U., Luch, A., 2018. Nanomaterials: certain aspects of application, risk assessment and risk communication. Arch. Toxicol. 92, 121–141. https://doi.org/10.1007/s00204-017-2144-1.
- Lee, S., Jun, B.-H., 2019. Silver Nanoparticles: Synthesis and Application for Nanomedicine. Int. J. Mol. Sci. 20, 865. https://doi.org/10.3390/ijms20040865.
- Li, R., Jay, J.A., Stenstrom, M.K., 2019. Fate of antibiotic resistance genes and antibioticresistant bacteria in water resource recovery facilities. Water Environ. Res. 91, 5–20. https://doi.org/10.1002/wer.1008.
- Lin, J.J., Lin, W.C., Da Li, S., Lin, C.Y., Hsu, S.H., 2013. Evaluation of the antibacterial activity and biocompatibility for silver nanoparticles immobilized on nano silicate platelets. ACS Appl. Mater. Interfaces. https://doi.org/10.1021/am302534k.
- Londono, S.C., Hartnett, H.E., Williams, L.B., 2017. Antibacterial activity of aluminum in clay from the Colombian Amazon. Environ. Sci. Technol. 51, 2401–2408. https://doi.org/10.1021/acs.est.6b04670.
- Lu, H., Wang, J., Stoller, M., Wang, T., Bao, Y., Hao, H., 2016. An Overview of Nanomaterials for Water and Wastewater Treatment. Adv. Mater. Sci. Eng. 2016, 1–10. https://doi.org/10.1155/2016/4964828.

- Luo, Y., Guo, W., Ngo, H.H., Nghiem, L.D., Hai, F.I., Zhang, J., Liang, S., Wang, X.C., 2014. A review on the occurrence of micropollutants in the aquatic environment and their fate and removal during wastewater treatment. Sci. Total Environ. 473–474, 619–641. https://doi.org/10.1016/j.scitotenv.2013.12.065.
- Magaña, S.M., Quintana, P., Aguilar, D.H., Toledo, J.A., Ángeles-Chávez, C., Cortés, M.A., León, L., Freile-Pelegrín, Y., López, T., Sánchez, R.M.T., 2008. Antibacterial activity of montmorillonites modified with silver. J. Mol. Catal. A Chem. 281, 192–199. https://doi.org/10.1016/j.molcata.2007.10.024.
- Pahlow, S., Meisel, S., Cialla-May, D., Weber, K., Rösch, P., Popp, J., 2015. Isolation and identification of bacteria by means of Raman spectroscopy. Adv. Drug Deliv. Rev. 89, 105–120. https://doi.org/10.1016/j.addr.2015.04.006.
- Pal, P., 2017. Nanotechnology in water treatment. In: Pal, P. (Ed.), Industrial Water Treatment Process Technology. Elsevier, pp. 513–536. https://doi.org/10.1016/B978-0-12-810391-3.00007-2.
- Prieto-Rodriguez, L., Miralles-Cuevas, S., Oller, I., Agüera, A., Puma, G.L., Malato, S., 2012. Treatment of emerging contaminants in wastewater treatment plants (WWTP) effluents by solar photocatalysis using low TiO2concentrations. J. Hazard. Mater. 211–212, 131–137. https://doi.org/10.1016/j.jhazmat.2011.09.008.
- Primm, T.P., Lucero, C.A., Falkinham, J.O., 2004. Health Impacts of Environmental Mycobacteria. Clin. Microbiol. Rev. 17, 98–106. https://doi.org/10.1128/CMR.17.1.98-106.2004.
- Quintero, R.I., Rodriguez, F., Bruna, J., Guarda, A., Galotto, M.J., 2013. Cellulose acetate butyrate nanocomposites with antimicrobial properties for food packaging. In: Packaging Technology and Science. John Wiley & Sons, Ltd, pp. 249–265. https://doi.org/10.1002/pts.1981.
- Salgot, M., Folch, M., 2018. Wastewater treatment and water reuse. Curr. Opin. Environ. Sci. Heal. 2, 64–74. https://doi.org/10.1016/j.coesh.2018.03.005
- Scandura, G., Ciriminna, R., Ozer, L.Y., Meneguzzo, F., Palmisano, G., Pagliaro, M., 2017. Antifouling and photocatalytic antibacterial activity of the AquaSun coating in seawater and related media. ACS Omega 2, 7568–7575. https://doi.org/10.1021/acsomega.7b01237.
- Sharma, V.K., Siskova, K.M., Zboril, R., Gardea-Torresdey, J.L., 2014. Organic-coated silver nanoparticles in biological and environmental conditions: Fate, stability and toxicity. Adv. Colloid Interf. Sci. 204, 15–34. https://doi.org/10.1016/j.cis.2013.12.002.
- Sheng, Z., Liu, Y., 2011. Effects of silver nanoparticles on wastewater biofilms. Water Res. 45, 6039–6050. https://doi.org/10.1016/j.watres.2011.08.065.
- Silvestre, C., Cimmino, S., Pezzuto, M., Marra, A., Ambrogi, V., Dexpert-Ghys, J., Verelst, M., Augier, S., Romano, I., Duraccio, D., 2013. Preparation and characterization of isotactic polypropylene/zinc oxide microcomposites with antibacterial activity. Polym. J. 45, 938–945. https://doi.org/10.1038/pj.2013.8.
- Sing, K.S.W., Everett, D.H., Haul, R.A.W., Moscou, L., Pierotti, R.A., Rouquerol, J., Siemieniewska, T., 1985. Reporting physisorption data for gas/solid systems with special reference to the determination of surface area and porosity. Pure Appl. Chem. 57, 603–619. https://doi.org/10.1351/pac198557040603.

- Su, H.-L., Lin, S.-H., Wei, J.-C., Pao, I.-C., Chiao, S.-H., Huang, C.-C., Lin, S.-Z., Lin, J.-J., 2011. Novel nanohybrids of silver particles on clay platelets for inhibiting silverresistant bacteria. PLoS One 6, e21125. https://doi.org/10.1371/journal.pone.0021125.
- Suppakul, P., 2016. Cinnamaldehyde and Eugenol. In: Antimicrobial Food Packaging. Elsevier, pp. 479–490. https://doi.org/10.1016/B978-0-12-800723-5.00039-5.
- Tilley, E., Lüthi, C., Morel, A., Zurbrügg, C., Schertenleib, R., 2014. Compendium of Sanitation Systems and Technologies. Eawag. Tran, Q.H., Nguyen, V.Q., Le, A.T., 2013. Silver nanoparticles: synthesis, properties, toxicology, applications and perspectives. Adv. Nat. Sci. Nanosci. Nanotechnol. 4, 033001. https://doi.org/10.1088/2043-6262/4/3/033001.
- Unuabonah, E.I., Ugwuja, C.G., Omorogie, M.O., Adewuyi, A., Oladoja, N.A., 2018. Clays for efficient disinfection of bacteria in water. Appl. Clay Sci. 151, 211–223. https://doi.org/10.1016/j.clay.2017.10.005.
- Vimbela, G.V., Ngo, S.M., Fraze, C., Yang, L., Stout, D.A., 2017. Antibacterial properties and toxicity from metallic nanomaterials. Int. J. Nanomedicine 12, 3941–3965. https://doi.org/10.2147/IJN.S134526.
- Wang, L.S., Wei, D. Bin, Wei, J., Hu, H.Y., 2007. Screening and estimating of toxicity formation with photobacterium bioassay during chlorine disinfection of wastewater. J. Hazard. Mater. 141, 289–294. https://doi.org/10.1016/j.jhazmat.2006.07.001.
- Wang, T., Zhang, D., Dai, L., Chen, Y., Dai, X., 2016. Effects of metal nanoparticles on methane production from waste-activated sludge and microorganism community shift in anaerobic granular sludge. Sci. Rep. 6, 25857. https://doi.org/10.1038/srep25857.
- Williams, L.B., 2017. Geomimicry: harnessing the antibacterial action of clays. Clay Miner. 52, 1–24. https://doi.org/10.1180/claymin.2017.052.1.01.
- Williams, A.C., Edwards, H.G.M., 1994. Fourier transform Raman spectroscopy of bacterial cell walls. J. Raman Spectrosc. 25, 673–677. https://doi.org/10.1002/jrs.1250250730.
- Williams, L.B., Metge, D.W., Eberl, D.D., Harvey, R.W., Turner, A.G., Prapaipong, P., Poret-Peterson, A.T., 2011. What makes a natural clay antibacterial? Environ. Sci. Technol. 45, 3768–3773. https://doi.org/10.1021/es1040688.
- Yang, Y., Zhang, C., Hu, Z., 2013. Impact of metallic and metal oxide nanoparticles on wastewater treatment and anaerobic digestion. Environ. Sci. Process. Impacts. https://doi.org/10.1039/c2em30655g.
- Yuan, Z., Chen, Y., Li, T., Yu, C.-P., 2013. Reaction of silver nanoparticles in the disinfection process. Chemosphere 93, 619–625. https://doi.org/10.1016/j.chemosphere.2013.06.010.
- Yuehua, H., Wei, S., Haipu, L., Xu, Z., 2004. Role of macromolecules in kaolinite flotation. Miner. Eng. 17, 1017–1022. https://doi.org/10.1016/j.mineng.2004.04.012.
- Zhou, Y., Kong, Y., Kundu, S., Cirillo, J.D., Liang, H., 2012. Antibacterial activities of gold and silver nanoparticles against Escherichia coli and bacillus Calmette-Guérin. J. Nanobiotechnol. 10, 19. https://doi.org/10.1186/1477-3155-10-19.